**Atmospheric
Chemistry
and Physics
Discussions**

NLC and the background atmosphere above ALOMAR

J. Fiedler, G. Baumgarten, U. Berger, P. Hoffmann, N. Kaifler, and F.-J. Lübken

Leibniz Institute of Atmospheric Physics at the Rostock University, Schloss-Str. 6, 18225 Kühlungsborn, Germany

Correspondence to: J. Fiedler (fiedler@iap-kborn.de)

ACPD

11, 5641–5679, 2011

NLC and background atmosphere

J. Fiedler et al.

Title Page

Abstract	Introduction
Conclusions	References
Tables	Figures

Back | Close

Full Screen / Esc

Printer-friendly Version

Interactive Discussion

Abstract

Noctilucent clouds (NLC) have been measured by the Rayleigh/Mie/Raman-lidar at the ALOMAR research facility in Northern Norway (69° N, 16° E). From 1997 to 2010 NLC were detected during more than 1850 h on 440 different days. Colocated MF-radar measurements and calculations with the Leibniz-Institute Middle Atmosphere (LIMA-) model are used to characterize the background atmosphere. Temperatures as well as horizontal winds at 83 km altitude show distinct differences during NLC compared to the absence of NLC. On seasonal mean it is colder and the winds are stronger westward when NLC are detected. The wind separation is a robust feature as it shows up in measurements as well as in model and it is consistent with the current understanding that lower temperatures support the existence of ice particles. For the whole 14-years data set there is no statistically significant relation between NLC occurrence and solar activity. On the other hand NLC occurrence and temperatures at 83 km show a significant anti-correlation, which suggests that the thermal state plays a major role for the existence of ice particles and dominates the pure Lyman-α influence on water vapor during certain years. We find the seasonal mean NLC altitudes to be correlated to both Lyman-α radiation and temperature. NLC above ALOMAR are strongly influenced by atmospheric tides. Diurnal and semidiurnal amplitudes and phases show partly pronounced year-to-year variations. In general, amplitudes as well as phases vary in a different manner. Amplitudes change by a factor of more than 3 and phases vary by up to 7 h. Such variability can impact NLC observations limited to fixed local times.

1 Introduction

More than 125 years ago unusual clouds, visible as twilight phenomena after sunset, were documented for the first time (Backhouse, 1885; Jesse, 1885; Leslie, 1885). While the surface of the Earth was already dark they appeared as striking glowing displays. The only explanation was illumination by the sun and it became clear that these clouds must be at exceptionally high altitudes. They were given the name noctilucent

clouds (NLC) and by optical triangulation the altitude was determined to be around 82 km (Jesse, 1896). Since the beginning the clouds attracted the interest of a growing number of observers and it was realized that the bluish-white displays reoccurred every summer. However, it took about 50 years until naked eye observations of NLC were
5 first summarized in a comprehensive work. Vestine (1934) showed that the maximum frequency of occurrence was about 10 days after summer solstice. Already in 1912 it was suggested that NLC are composed of ice particles (Wegener, 1912), which was finally proven by Hervig et al. (2001). NLC displays often show a rich variability, even on scales of few kilometres, which provides information about dynamic processes like hor-
10 izontal wind and wave motions in their environment (Witt, 1962). About 80 years after the initial observations the available information was compiled by Fogle and Haurwitz (1966). They pointed out that a relation between increased NLC activity and reduced solar activity, already suggested by Vestine (1934), cannot reliably be answered until a larger data basis, covering a few sunspot cycles, will be available. Around that time
15 the two longest-lasting NLC time series based on visual observations of the number of nights with cloud displays per season started: NW-Europe (Gadsden, 1989) and Moscow (Romejko et al., 2003). They now cover more than 4 decades.

Starting with the OGO-6 satellite, NLC are also detected from space (Donahue et al., 1972) and were later called polar mesospheric clouds (PMC). As both names
20 refer to the same phenomenon we will use the original notation (NLC) throughout the manuscript. Since 1979 the solar backscattered ultraviolet instruments (SBUV) on-board the NOAA satellites, operating from sun-synchronous orbits, observe the clouds on regular basis by detecting an enhanced Earth albedo (Thomas et al., 1991).

There is evidence that NLC consist of ice particles and are bound to very low tem-
25 peratures around and below 150 K in combination with water vapor mixing ratios of only a few ppmv (e.g., Turco et al., 1982; Lübken et al., 1996; Berger and von Zahn, 2002; Rapp and Thomas, 2006). They are extremely sensitive to changes of these atmospheric background parameters, which are difficult to monitor with high accuracy, and may therefore serve as indicators for long-term changes.

For both the NW-Europe and SBUV data sets, a mean anti-correlation between solar activity and NLC occurrence was shown (Kirkwood et al., 2008; Shettle et al., 2009). The SBUV time series shows this anti-correlation also with respect to NLC brightness and additionally an increasing trend of both occurrence and brightness (DeLand et al.,
5   2007; Shettle et al., 2009). The robustness of these trends was disputed, partly based on the altitude of the clouds which seems to be unchanged since more the 100 years (von Zahn, 2003; Thomas et al., 2003). The virtually constant NLC altitudes were recently investigated by lidar observations covering roughly one decade (Fiedler et al., 2009).

10 Laser optical remote sensing is a precise method to observe NLC since about 20 years. Lidar instruments have shown the variability of cloud occurrence and layer parameters on time scales from minutes to decades, including gravity wave, tidal and solar cycle variations (e.g., Thayer et al., 2003; Chu et al., 2003; Höffner et al., 2003; Fiedler et al., 2005; Gerding et al., 2007; Klekociuk et al., 2008). Multi-wavelength and
15 polarization techniques were successfully applied for NLC particle size and shape determinations (von Cossart et al., 1999; Alpers et al., 2000; Baumgarten et al., 2008, 2002).

A perfect instrument for NLC research would combine high accuracy with high temporal and spatial resolution during simultaneously global temporal as well as spatial
20 coverage of the Earth. Comparing ground-based lidar and satellite techniques it is obvious that each has advantages and disadvantages. Lidars maintain high temporal and vertical resolution as well as accuracy, but suffer from interruptions as they depend on the weather conditions and are limited to observations at fixed geographic locations. Satellite instruments can provide a global spatial mapping independent of tropospheric
25 conditions, but only at fixed local times when on sun-synchronous orbits. Even when they precess, it takes weeks to cover a complete range at all local times.

The question suggesting itself is, how reliable does a measurement represents the true state? In the following we will investigate this subject for our lidar at the Arctic station ALOMAR. The observation of NLC at this geographic location began already

in 1989 and continues to the present day (Hansen et al., 1989; Langer et al., 1995; Nussbaumer et al., 1996). We investigate a continuous time series starting 1997 which is the most extensive NLC data set obtained by lidar so far. Using model and radar data we will characterize the background atmosphere during our NLC observations and use model temperatures as proxy for the lidar sampling quality. A further topic are year-to-year variations of tidal NLC parameters and possible implications on satellite-based time series.

2 Data basis

For our investigations we use data obtained by lidar, radar, and model for the location of the Arctic Lidar Observatory for Middle Atmosphere Research (ALOMAR) facility in Northern Norway at 69° N, 16° E.

2.1 Lidar

The ALOMAR Rayleigh/Mie/Raman-(RMR-) lidar is designed to operate on a routine basis throughout the year (von Zahn et al., 2000) and optimized for the detection of NLC. A combination of spectral highly stable laser transmitter and strong spatial and spectral filtering at the receiving side allows NLC observations during highest solar elevations throughout the Arctic summer. The detector records laser photons backscattered from air molecules and NLC particles as function of altitude z as well as sunlight scattered by the atmosphere. After background subtraction the signal is converted to volume backscatter coefficient of NLC particles:

$$\beta_{\mathrm{NLC}}(z) = (R(z) - 1) \times \beta_M(z) \tag{1}$$

using the backscatter ratio $R(z)$ as measure for the presence of aerosol particles, which is defined as the ratio of the measured total signal to the molecular signal $\beta_M(z)$. From the altitude profile $\beta_{\mathrm{NLC}}(z)$ we determine the maximum value β_{max}, the total backscatter coefficient β_{tot} (integral over the vertical layer extension) and the centroid altitude

Full Screen / Esc

Printer-friendly Version

Interactive Discussion

z_c. For our investigations we use data obtained at 532 nm laser wavelength with an altitude/time resolution of 150 m/14 min. Detailed information regarding the data processing is given in Fiedler et al. (2009).

For better readability we will use the term "brightness" as synonym for β_{max} as well as β_{tot} because the volume backscatter coefficient closely relates to the brightness which a human observer would experience. Values of β_{max} will be given in units of 10^{-10} m^{-1} sr^{-1}, unless otherwise stated.

Signal and measurement uncertainty (determined from Poisson statistics of the photon counting process) at a given altitude depend on various processes, like i.e. atmospheric transmission and system performance, and are consequently subject of variations from minutes to years. We introduce two data subsets to maintain sensitivity limits for NLC detection, which are determined by the mean measurement uncertainty $\Delta\beta_{NLC}(z)$ in the altitude range from 80 to 90 km: the long-term data set contains only measurements with $\Delta\beta_{NLC}(z) < 4\times10^{-10}$ m^{-1} sr^{-1}, whereas the high-sensitivity data set is limited to measurements with $\Delta\beta_{NLC}(z) < 1\times10^{-10}$ m^{-1} sr^{-1}. Figure 1 shows the measurement times of the data subsets in comparison to the entire measurement time of the lidar. In total the signal quality is sufficient to determine potential NLC having $\beta_{max} > 4$ (>1) during 97% (59%) of the time. Since 2006 both data subsets cover nearly the same amount of data which shows the increased sensitivity of the detection system achieved by replacing photomultiplier tubes with avalanche photodiodes.

From 1997 to 2010 the entire data set consists of ∼4340 measurement hours where NLC were detected during ∼1865 h on ∼440 different days. In the following sections we will use three lower brightness limits to classify NLC, which are used in combination with the appropriated data subset: $\beta_{max} > 1$ (=high-sensitivity limit, 63% of all NLC detections within the high-sensitivity data set), $\beta_{max} > 4$ (=long-term limit, 55% of all NLC detections within the long-term data set), $\beta_{max} > 13$ (=strong clouds, 16% of all NLC detections within the long-term data set).

2.2 Radar

The ALOMAR MF-radar is designed for investigations of the dynamics of the mesosphere and lower thermosphere. It has continuously provided horizontal winds at altitudes between 70 and 94 km since 1998 using the full correlation analysis method. The radar operates at 1.98 MHz and uses a vertically pointing wide beam antenna for the transmission of radio wave pulses of 4 km length. The atmospheric returns are received by three crossed horizontal dipoles arranged in an equilateral triangle. More details are given in Singer et al. (1997). Wind values are derived with oversampling in height steps of 2 km and with a time resolution of 3 min. We will use here hourly mean winds to characterize the dynamics at NLC altitudes.

2.3 Model

The Leibniz-Institute Middle Atmosphere (LIMA-) model is a circulation model of the middle atmosphere with special focus on the thermal structure around mesopause altitudes (Berger, 2008). LIMA is a fully non-linear, global, and 3-d Eulerian grid-point model which extends from the ground to the lower thermosphere (0–150 km) taking into account major processes of dynamics, radiation, chemistry, and transport. It implements a triangular horizontal grid structure with 41804 grid points in every horizontal layer ($\Delta x \sim \Delta y \sim 110$ km), and the adaptation of tropospheric and lower stratospheric data from ECMWF/ERA-40 up to an altitude of 30 km every 6 h. This introduces a coupling of the model results in the mesopause region to the wave activity from planetary to tidal to gravity wave scales in tropo- and stratosphere. The current version of LIMA also includes the spectral solar irradiance relative to Lyman-α variability (taken from http://lasp.colorado.edu/lisird/lya/) as well as solar heating processes in the ultraviolet. We will use LIMA results of temperature and horizontal winds for characterization of the background atmosphere. The time resolution is 1 h, until otherwise stated.

3 Year-to-year variations and sampling quality

For ground-based lidar measurements clear sky is needed and hence they depend on the weather conditions. For this reason a single year of our NLC data base is a rather patchy time series representing clear sky conditions above ALOMAR. Between 1 June
5 and 15 August the total measurement times cover about 25% of the maximum possible time during good years and drop down to about 7% during bad years. This could bias the statistical robustness of long-term time series because all cloud parameters show variations with season and local time. Fiedler et al. (2009) investigated the reliability of the NLC occurrence time series by randomly choosing data subsets as well as taking
10 into account the conservation tendency of geophysical data. The results confirmed the general year-to-year variation pattern obtained from the entire data set.

Here we use a different method to estimate the impact of unequal sampling on the seasonal mean values of the NLC parameters (occurrence, altitude, brightness). The 14-years mean seasonal and local time variations of a parameter are used to calculate
15 the expected seasonal mean value for each year using the actual observation times of the particular year. The deviation between expected and actually measured seasonal mean values is regarded as sampling quality.

To characterize the mean variations we use updated values, covering the range from 1997 to 2010, for the parametrizations given in Fiedler et al. (2005, 2009). The sea-
20 sonal variations are characterized by third-order polynomial fits. Local time variations are described by harmonic fits using periods of 24, 12, 8 and 6 h:

$$\text{DOY}(d) = a_0 + a_1 d + a_2 d^2 + a_3 d^3 \tag{2}$$

$$\text{LT}(t) = A_0 + A_{24}\cos\left[\frac{2\pi}{24}(t - \phi_{24})\right] + A_{12}\cos\left[\frac{2\pi}{12}(t - \phi_{12})\right] + \dots \tag{3}$$

where a are the fit coefficients, d is day relative to solstice, A_0 is the mean value, A and
25 ϕ are the amplitudes and phases of the wave components and t is local time in hours.

The following method is applied to each NLC parameter, because occurrence, altitude and brightness show different variation patterns over season as well as local time. At first the two individual fits (DOY, LT) are calculated and normalized to their mean values $\overline{\text{DOY}}$ and $\overline{\text{LT}}$. This yields the relative variation of the NLC parameter. Given a full temporal sampling of a fit curve (76 days per season, 24 h per day), the resulting mean value would be equal to one. Then for each day and hour of the season the contributions of seasonal and local time variations are combined by multiplying daily and hourly relative variations:

$$\text{FIT}_{\text{rel}}(d,t) = \frac{\text{DOY}(d)}{\overline{\text{DOY}}} \times \frac{\text{LT}(t)}{\overline{\text{LT}}} \qquad (4)$$

Again, the mean value of this overall fit curve FIT_{rel} equals one. The result is shown in Fig. 2. We determine the effect of a non-perfect sampling in each year as follows: we take the FIT_{rel}-values from Fig. 2 at the measurement times in a specific year and determine the mean of these FIT_{rel}-values, which we call the "relative sampling factor" RSF. This factor is an estimate of the bias introduced by the sampling effect and is shown in Fig. 3 (left panels). For example, RSF = 1.1 for the occurrence frequency in 2004 means that the mean occurrence frequency calculated in that year is probably overestimated by 10% due to sampling effects. Note that this method assumes temporal variations of same type during each year which is doubtless only an approximation of the (unknown) actual conditions.

For the long-term data set the uncertainties introduced by unequal sampling are roughly ±10% for occurrence and brightness. The uncertainty of NLC altitudes is smaller by a factor of ∼100, which is caused by the small altitude variability over season and local time. The uncertainties for the high-sensitivity data set are generally larger because of the reduced amount of data. We notice that the years showing the worst sampling quality are not identical for each parameter. While in 2005 the occurrence was overestimated by 25%, the values for altitude and brightness are rather small. On the other hand RSF for altitude shows maxima during 2001 and 2002. This

Full Screen / Esc

Printer-friendly Version

Interactive Discussion

is caused by the different variation patterns of the parameters over season and local time shown in Fig. 2. It is interesting to note that years with a small amount of data do not necessarily show a bad sampling quality. The measurement time in 2006 was only 36% compared to 2007 but the uncertainties of all parameters introduced by unequal sampling hardly differ from each other. The sampling qualities of both data sets (long-term and high-sensitivity) are almost identical since 2006, which is caused by technical improvements of the lidar system, and differ from each other in the years before.

Figure 3 shows on the right panels the time series of NLC occurrence, altitude and brightness, each for clouds above the high-sensitivity limit ($\beta_{max} > 1$), above the long-term limit ($\beta_{max} > 4$) as well as strong clouds ($\beta_{max} > 13$). The solid curves result from the regular data processing, the dashed curves are corrected regarding the sampling quality by normalization to RSF-values. It turns out that for each NLC parameter the general variation patterns of the long-term data set are not significantly affected by the sampling. The deviations are larger for the high-sensitivity data set. Until 2003 the confidence limits of the NLC occurrence for clouds having $\beta_{max} > 1$ are enhanced due to the weak measurement statistics within the high-sensitivity data set.

The general variation patterns are fairly similar for the three brightness classes, but at different mean levels. A detailed discussion of the year-to-year variability until 2007 can be found in Fiedler et al. (2009). We conclude that the sampling influence on our measurements is rather weak and will use the results without corrections during the next sections.

4 Local time variations

The mean diurnal variations of NLC occurrence, altitude and brightness over 14 years are shown in Fig. 4. All three time series, i.e. clouds above the high-sensitivity limit ($\beta_{max} > 1$), above the long-term limit ($\beta_{max} > 4$) as well as strong clouds ($\beta_{max} > 13$), show similar patterns but on different mean levels. There are pronounced persistent features indicating strong tidal influences on ice particles above ALOMAR, which has been shown earlier (Fiedler et al., 2005). NLC occur most frequently in the morning

Title Page

Abstract | Introduction

Conclusions | References

Tables | Figures

◄ | ►|

◄ | ►

Back | Close

Full Screen / Esc

Printer-friendly Version

Interactive Discussion

hours and most seldom around noon. Occurrence differences during the day can reach a factor of 8, depending on the brightness limit. The altitude is lowest around 8 LT and highest during midnight and the early afternoon, the variability range during day is about 1 km. NLC are generally less bright from noon to midnight compared to the first
5 half of the day.

We have investigated the year-to-year variations of the tidal components. To enhance the statistical robustness we calculated running means of the NLC parameters, covering three years each. Harmonic fits to the data have been done using the method described in Sect. 3. Fit coefficients are determined considering errors of the
10 hourly means by applying a Levenberg-Marquardt-algorithm. The so-called reduced Chi-square value describes the quality of least squares fits and should be around one. The mean value of all our fits is 1.3 ± 0.8 which indicates that fit model and data are adequate to each other. The amplitudes of 8 and 6 h periods are generally smaller than those for 24 and 12 h. Shorter periods could be caused by geophysics, such as
15 wave-wave interactions of tidal components or gravity waves, but may additionally be impacted by a limited sampling. In the following we will investigate only the diurnal and semidiurnal components.

Figure 5 shows for clouds above the long-term limit the year-to-year variations of amplitudes and phases for 24- and 12-hour periods of occurrence, altitude and brightness.
20 Data points are plotted at the center of the corresponding 3 years range.

The diurnal and semidiurnal phases of the NLC occurrence are quite stable around 4 LT, which is the underlying reason for the NLC recurrence maximum in the morning hours. The diurnal amplitude is stronger than the semidiurnal during each year and decreases by about 50% from 1999 to 2007.
25 The phases of the NLC altitude are separated by about 6 h and vary by only about 3 h during 14 years. The amplitudes of both components increase more or less steadily by about 100% until 2006 and decrease again thereafter. During half of all years diurnal an semidiurnal amplitudes are approximately equal, the other years are dominated by the semidiurnal component.

For brightness (β_{max}) the semidiurnal phase is almost constant around 6:30 LT until 2004 and decreases thereafter by about 4.5 h. The diurnal phase shows a nearly monotonic increase from 1998 to 2009 by about 7 h. This phase shift is a striking feature of the time series and is also visible when using β_{tot} for characterization of the NLC brightness. The anti-correlation of the tidal oscillations of altitude and brightness (Fiedler et al., 2005) deteriorates from the first to the second half of the 14-years data set (r = −0.77 from 1997–2003, r = −0.68 from 2004–2010), but is still significant on 99% level. The diurnal amplitude decreases strongly after 2005. The semidiurnal amplitude shows maximum values at 1998 and 2006 and a deep distinct minimum in between, which is centered around 2001.

In summary we note that some tidal parameters are fairly constant in time (e.g. 24 h phase of occurrence), whereas other vary substantially (e.g. 12 h amplitude of brightness).

5 Atmospheric background conditions during observations

Ice particles in the mesopause region react sensitive to their atmospheric background, especially temperature and water vapour. This has been shown by numerous models of different kind. Water vapour provided, temperature turns out to be the main driving parameter for the existence and properties of NLC. Seasonal mean temperature variations at NLC altitudes are calculated to be up to 3 K over a solar cycle (Schmidt et al., 2006; Marsh et al., 2007). Over the summer season temperatures have been measured to change by about 7 K (Lübken, 1999). Gravity wave activity can cause variations of ∼15 K within a few hours (Rauthe et al., 2006).

In Berger (2008) it was shown that LIMA produces reasonable temperatures on annual scales, based on daily means. Here we investigate how results from the LIMA-model are related to NLC observations above ALOMAR. Figure 6 shows the NLC time series obtained during three days of continuous lidar measurements early in July 2005 as well as the calculated fields for temperature and horizontal winds.

Time resolution for both RMR-lidar and LIMA data is ∼ 150 seconds. To see more details, for temperature and zonal wind also the deviations from the three days mean altitude profiles are shown. At 83 km the temperature mean (range) is about 148 K (8 K). The zonal wind is always westward directed with a mean (range) of about -44 m s^{-1}
5 (35 m s^{-1}). The meridional wind changes direction in the course of the day between about -15 m s^{-1} and +10 m s^{-1}, resulting in a small mean value of -0.5 m s^{-1}. To link the observations with the model, the NLC contours for a brightness of $\beta_{max} = 4$ are plotted on top of the LIMA results.

As can be seen, within these three days NLC occur nearly solely during the cold
10 phases of the temperature anomalies and mostly during periods of enhanced westward winds. For meridional winds the picture is ambiguous as NLC were observed both during southward and northward winds.

In a next step we use the whole data basis of RMR-lidar measurements from 1997 to 2010 in order to check if the agreement found above is statistically robust. For that,
15 seasonal mean values of temperature and horizontal winds at 83 km altitude above ALOMAR are calculated with LIMA for times of confirmed absence as well as presence ($\beta_{max} > 4$) of NLC within the lidar long-term data set. LIMA results are based on hourly means. The result is shown in Fig. 7. During each single year it is colder and the westward winds have been stronger during NLC observations compared to the
20 absence of NLC. This separation also shows for the meridional wind, but not during all years.

Average values (standard deviations) over 14 years for temperature, zonal and meridional wind at 83 km during NLC presence ($\beta_{max} > 4$) are 147.6 K (2.3 K), −44.2 m s^{-1} (11.0 m s^{-1}) and −3.3 m s^{-1} (9.4 m s^{-1}), respectively. The 14-years
25 mean differences between NLC presence and absence are −2.0 K for temperature, −9.1 m s^{-1} for zonal wind and −2.5 m s^{-1} for meridional wind. The pronounced differences between NLC presence and absence are also visible with respect to local time for temperature and zonal wind, and to a lesser extent for the meridional wind (not shown here).

NLC and background atmosphere

J. Fiedler et al.

◄◄ | ►►

◄ | ►

Back | Close

Full Screen / Esc

Printer-friendly Version

Interactive Discussion

Figure 7 also shows horizontal winds obtained by the ALOMAR MF-radar, which determines mesospheric winds since 1999 on a regular basis. The seasonal means have been processed in the same way like the LIMA winds, namely based on hourly means and sorted for NLC yes/no cases. Average values (standard deviations) over 12 years for zonal and meridional wind at 83 km during NLC presence ($\beta_{max} > 4$) are −27.6 m s^{-1} (14.8 m s^{-1}) and −6.9 m s^{-1} (15.0 m s^{-1}), respectively. The 12-years mean differences between NLC presence and absence are −10.5 m s^{-1} for zonal wind and −4.6 m s^{-1} for meridional wind. During particular years the zonal wind during NLC absence can remarkably deviate from the usual summer westward wind regime.

Firstly we note that geophysical variabilities are in the order of, or even larger than, the differences between NLC presence and absence. The meridional wind shows a particularly high variability caused by the direction reversals during the day. Secondly, absolute wind values are different for LIMA and MF-radar, especially for the zonal wind, which however does not matter for our considerations. Much more important, the pronounced pattern of stronger westward winds during NLC presence versus absence is in evidence. Like in the LIMA results, this is to a lesser extent visible in the meridional winds. Differences in year-to-year wind variations between model and measurement are at least partly caused by unequal time coverage as the atmospheric scatter conditions for the MF-radar method are not always sufficient for wind determinations.

We conclude that the wind separation into NLC yes/no cases is a robust feature as it shows up in measurement as well as model. The feature of lower temperatures calculated by LIMA during measured NLC presence compared to absence appears plausible from the ice particles point of view. In combination with the wind results we conclude that LIMA seems to reproduce the background atmosphere to a sufficient degree even on hourly resolution.

6 Discussion

In Sect. 5 we have shown that LIMA produces reasonable results on hourly basis, namely meaningful temperature differences and by measurements approved wind differences for NLC presence/absence in the RMR-lidar data.

The relation between temperature and NLC seems plausible as lower temperatures support the existence of ice particles. Southward winds will usually transport the particles from colder regions further north towards ALOMAR (Berger and von Zahn, 2007). However, the relationship between stronger westward winds and enhanced NLC occurrence is not readily obvious. We note that in Fig. 6 the anomalies of temperature and zonal wind are in phase most of the time, i.e. lower temperatures coincide with enhanced westward winds. Processes influencing both temperature and winds could be related to planetary waves. Stronger zonal winds could also be connected with an enhanced residual circulation (vertical winds) which produces lower temperatures by adiabatic cooling. Another possibility relates to gravity wave filtering. Assuming the zonal wind variations covering also stratosphere/lower mesosphere, they could change the gravity wave spectrum reaching the mesopause region. This can finally affect the NLC existence, cf. Rapp et al. (2002); Chandran et al. (2010). However, such investigations are beyond the scope of this work.

The temperature and horizontal wind differences between presence/absence of NLC show that the local atmospheric conditions considerably contribute to the existence of ice particles. This is supported by model calculations. Berger and von Zahn (2007) showed that the most likely transport time of an NLC particle from nucleation to a radius larger than 50 nm is about 30 h. Particle trajectories calculated by LIMA/ICE additionally indicate that especially the last 6 h of the particle lifetime are essential for maximum ice growth (Kiliani, personal communication, 2010).

The reproduction of the background atmosphere by LIMA should also arise in tidal variations. Figure 8 shows the diurnal variations of NLC occurrence ($\beta_{max} > 4$) and temperatures at 83 km altitude during times of lidar measurements for the integrated data

Title Page

Abstract | Introduction

Conclusions | References

Tables | Figures

◄ | ►|

◄ | ►

Back | Close

Full Screen / Esc

Printer-friendly Version

Interactive Discussion

sets from 1997 to 2010. The anti-correlation is almost perfect ($r = -0.96$, 99%-level). The mean temperature variation during the day is 3.4 K. Stevens et al. (2010) reported comparable strong relations between temperature at 83 km and ice particles. Using a global numerical weather prediction system that assimilates satellite temperature and water vapor observations from ground to 90 km altitude, they found the migrating diurnal temperature tide at 69° N to control the variation of NLC total ice water content over the diurnal cycle.

6.1 Sampling quality

An important topic for interpretation of time series which do not cover all local times is, how the measured value differs from the "true" one. Inherently this question cannot be answered from itself. Comparing actual results with the long-term mean behavior is one approach, which we have used in Sect. 3. The result showed that the influence of unequal temporal sampling over season and diurnal cycle is rather small when using the mean seasonal and diurnal variations of 14 years for reference. Another possibility is the usage of a different parameter, which is strongly related to the virtual one and additionally always available, as proxy for missing measurements. We will here use the LIMA temperatures at 83 km altitude as proxy for times when we lack lidar measurements to investigate the sampling quality regarding the time dependent temperature field above ALOMAR. Seasonal means from LIMA obtained solely for hours with lidar measurements are compared to entire means from 1 June to 15 August. The result is shown in Fig. 9. For the long-term data set the deviations from the entire seasonal means range between +0.5 K and −0.9 K. During each individual year these values are smaller than the ones resulting from the NLC yes/no separation, c.f. Fig. 7. The 14-years mean deviation is close to zero ($-0.09\,\text{K} \pm 0.12\,\text{K}$). The deviations for the high-sensitivity data set are larger during the first years due to the weaker measurement statistics. The 14-years mean deviation is $-0.31\,\text{K} \pm 0.13\,\text{K}$. Despite the different amount of measurement hours the deviations for 2006 and 2007 are nearly identical,

cf. Sect. 3. Generally we find no significant correlation between sampling quality and NLC occurrence when using LIMA temperatures above ALOMAR as proxy.

6.2 Tidal parameters

We find minimum values for the semidiurnal amplitude of NLC brightness during solar maximum (2001–2003), cf. Fig. 5. The correlation coefficient for the time range from 1998–2007 is −0.88, which indicates sufficient significance even when considering the 3-years running mean filter. There are virtually no investigations regarding the inter-relation between solar radiation and semidiurnal tides in the polar mesopause region. Randel et al. (2006) reported a sudden decrease of tropical stratospheric water va-por, tropopause temperature and ozone content starting 2001, which is explained by increasing Brewer-Dobson circulation. This could enhance extratropical stratospheric ozone which may be linked to increasing amplitudes of the semidiurnal tidal compo-nent. To what extent this might be relevant for polar latitudes remains speculation.

Satellite instruments usually operate from sun synchronous orbits and hence ob-serve NLC at two fixed local times, representing the ascending and descending nodes of the orbit. For the last three satellites contributing to the SBUV time series these are approx. 4 LT (NOAA-16/18), 12 LT (NOAA-16/17/18) and 21 LT (NOAA-17) around the latitude of ALOMAR. Additionally the orbit might shift over the lifetime of the satellite, e.g. NOAA-14 by 7 h (DeLand et al., 2007). For a precise detection of small trends the local time variation of NLC parameters is necessary to consider. DeLand et al. (2007) and Shettle et al. (2009) adjusted brightness (albedo) and occurrence frequency de-rived from SBUV measurements using a method which qualitatively reflects the tidal variability patterns observed above ALOMAR (Fiedler et al., 2005). However, our data set shows that amplitudes as well as phases of NLC occurrence and brightness are not constant over the years. They rather vary in a different manner: amplitudes can change by a factor of more than 3 and phases show changes of up to 7 h. To estimate the impact of this variability, we have reconstructed the occurrence and brightness time series from harmonic fits (24- and 12-hours oscillations only) for single local times. To

account for phase shifts, two data sets were reconstructed: one for the actual phases as shown in Fig. 5, the other one for identical (from 1997) phases during each year. The results are shown in Fig. 10 and Fig. 11 for 4, 12 and 21 LT in comparison with the time series containing all local times. We show here β_{tot} for the brightness as it repre-

5   sents the integrated signal over the vertical cloud extension which compares better to satellite observations than the peak signal (β_{max}).

As expected the time series show different mean levels, depending on local time. Additionally the year-to-year variations for single local times of occurrence and brightness differ from the overall curves. Also the 14-years-tendency (linear regression) can

10 be different for each local time.

For example the 4 LT occurrence time series, for actual as well as fixed phases, shows a decreasing behaviour which is not present in the overall curve containing all local times. On the other hand, the 12 LT occurrence time series for fixed phases tends to increase during the same time period.

15 The 12 LT brightness time series for the actual phases increases more or less steadily over the 14 years by a factor of 2.5. It differs substantially from the overall variation pattern when taking into account all local times.

In general, time series obtained at single local times can differ considerably from the ones containing the full diurnal cycle. In addition phase shifts change the seasonal

20 means by up to 100% during particular years and may alter the year-to-year variation patterns.

6.3   Correlations

Figure 12 shows the correlation between NLC occurrence from lidar and solar activity and temperature at 83 km from LIMA, respectively. Taking into account the whole time

25 series from 1997 to 2010, we find no significant anti-correlation between occurrence and solar activity. When removing the years 2005–2008 from the analysis the anti-correlation becomes significant on 95% level. During these years cloud occurrence and Lyman-α radiation were almost in-phase. On the other hand the anti-correlation

Printer-friendly Version

Interactive Discussion

between NLC occurrence and temperature is significant for the whole data set, and is even improving to 99% level when removing the single outlier 1998. This suggests that thermal conditions play a major role for the existence of ice particles, and dominate the pure Lyman-α influence on water vapor during certain years. This is supported by mesospheric water vapor measurements with a microwave instrument at ALOMAR. Hartogh et al. (2010) find during summer generally decreasing H_2O mixing ratios between 1996 and 2006 up to an altitude of 80 km, which is the uppermost altitude available from the instrument. The overall decrease during these 11 years is 15% in contrast to only 4.5% decrease between solar minimum and maximum due to the sensitivity of H_2O to Lyman-α radiation.

Table 1 gives an overview of several correlations investigated. The NLC brightness is anti-correlated to Lyman-α and shows no interrelationship to temperature. The altitude is positively correlated to both Lyman-α and temperature.

Lübken et al. (2009) investigated for 46 years (1961–2008) the seasonal mean NLC parameter sensitivity to solar activity and temperature using a model for both background atmosphere and ice particles (LIMA/Ice). In general we find comparable relationships, here for observed NLC. Weaker or even no correlations with respect to Lyman-α in Lübken et al. (2009) are probably caused by the missing solar cycle influence on temperature in their model version. Hence the exclusive solar cycle dependence originated from the assimilated ECMWF data. However, it is interesting that our data does not show a correlation between observed NLC brightness and modelled temperature, while there is a significant anti-correlation present for the modelled NLC (c.f. Lübken et al., 2009). In our data set the altitude sensitivity to temperature at 83 km is $+ 0.19\,\mathrm{km\,K^{-1}}$ (year 1998 removed), which is slightly smaller than calculated by different models: CARMA: $+0.25..+0.53$ (Lübken et al., 2007), LIMA/Ice: $+0.26$ (Lübken et al., 2009). However, these values do not contain the Lyman-α influence on the mesopause region. Our measured NLC altitudes show correlations to both Lyman-α and temperature. At the same time Lyman-α and temperature show no significant relationship over the 14 years. Therefore it is possible that Lyman-α masks the pure

temperature influence which in turn could explain the lower altitude sensitivity to temperature in our data set.

It appears complex to determine which part of the NLC variation is caused by solar activity, as solar radiation acts on both water vapor and temperature. Additionally the ice particles are modulated by atmospheric dynamics which altogether results into considerable natural variability.

7 Conclusions

We presented results from a multi-year NLC data set obtained by ground-based lidar at ALOMAR. The time series covers 14 years, starting 1997, and contains ~1865 h NLC detections during a total of ~4340 measurement hours. ALOMAR MF-radar and LIMA-model data were used to characterize the background atmosphere during lidar measurements.

When using atmospheric data solely determined for hours with lidar measurements and sorted for NLC yes/no cases we find a clear separation of seasonal mean temperature and horizontal winds at 83 km altitude: During each single year it was colder and the winds have been stronger westward during NLC observations compared to the absence of NLC. This separation is also visible for the meridional wind, but not during all years. 14-years mean differences between NLC presence and absence are -2 K for temperature, $-9\ldots-10$ m s^{-1} for zonal wind and $-2\ldots-5$ m s^{-1} for meridional wind. The wind separation is a robust feature as it shows up in measurement as well as model. The temperature separation seems plausible as lower temperatures support the existence of ice particles. We conclude that the LIMA-model is able to reproduce the background atmosphere to a sufficient degree on hourly resolution, at least on a statistical average over the NLC season.

The lidar sampling quality during each year was investigated regarding the multi-year mean diurnal and seasonal variations of NLC occurrence, altitude and brightness. It turned out that for each NLC parameter the general variation patterns of the long-term

data set are not significantly affected by the sampling. From the comparison of yearly mean temperatures calculated by LIMA solely for lidar measurement hours with entire means over the NLC season we follow that our NLC time series is most likely not biased by different sampling of the temperature structure at NLC altitudes.

We find no statistically significant relation between NLC occurrence and solar activity when using the whole time series from 1997 to 2010. The reason is, that between 2005 and 2008 cloud occurrence and Lyman-α radiation were almost in-phase, contrary to the other years. On the other hand the relationship to local temperature at NLC altitudes as calculated by LIMA is much stronger: The anti-correlation between NLC occurrence and temperature is significant for the whole data set, and is even improving to 99% level when removing the single outlier 1998. This suggests that thermal conditions play a major role for the existence of ice particles which dominates the pure Lyman-α influence on water vapor during certain years. We find the seasonal mean NLC altitudes to be correlated to both Lyman-α radiation and temperature. The sensitivity to temperature at 83 km is +0.19 km K^{-1} (year 1998 removed).

Our data set shows pronounced persistent variations of NLC occurrence, altitude and brightness with local time, which indicates a strong tidal influence on ice particles above ALOMAR. Depending on the parameter, diurnal and semidiurnal amplitudes and phases have different and partly strong year-to-year variations. Most striking features are shown by the NLC brightness: The semidiurnal amplitude has very low values during solar maximum and is over a period of 10 years significantly anti-correlated to Lyman-α radiation. The diurnal phase increases monotonic over the whole time series. In general, amplitudes as well as phases of NLC parameters are not constant over the years. They rather vary in a different manner, amplitudes can change by a factor of more than 3 and phases show changes up to 7 h. Such year-to-year variability can impact time series generated from observations at fixed local times, like obtained from sun-synchronous satellite orbits.

References

Alpers, M., Gerding, M., Höffner, J., and von Zahn, U.: NLC particle properties from a five-color lidar observation at 54° N, J. Geophys. Res., 105, 12235–12240, doi:10.1029/2000JD900132, 2000. 5644

Backhouse, T. W.: The luminous cirrus clouds of June and July, Meteorol. Mag., 20, p. 133, 1885. 5642

Baumgarten, G., Fricke, K. H., and von Cossart, G.: Investigation of the shape of noctilucent cloud particles by polarization lidar technique, Geophys. Res. Lett., 29(13), 1630, doi:10.1029/2001GL013877, 2002. 5644

Baumgarten, G., Fiedler, J., Lübken, F.-J., and von Cossart, G.: Particle properties and water content of noctilucent clouds and their interannual variation, J. Geophys. Res., 113, D06203, doi:10.1029/2007JD008884, 2008. 5644

Berger, U.: Modeling of middle atmosphere dynamics with LIMA, J. Atmos. Solar Terr. Phys., 1170–1200, doi:10.1016/j.jastp.2008.02.004, 2008. 5647, 5652

Berger, U. and von Zahn, U.: Icy particles in the summer mesopause region: Three-dimensional modeling of their environment and two-dimensional modeling of their transport, J. Geophys. Res., 107(A11), 1366, doi:10.1029/2001JA000316, 2002. 5643

Berger, U. and von Zahn, U.: Three-dimensional modeling of the trajectories of visible noctilucent cloud particles: An indication of particle nucleation well below the mesopause, J. Geophys. Res., 112, D16204, doi:10.1029/2006JD008106, 2007. 5655

Chandran, A., Rush, D. W., Merkel, A. W., Palo, S. E., Thomas, G. E., Taylor, M. J., Bailey, S. M., and Russell III, J. M. R.: Polar mesospheric cloud structures observed from the cloud imaging and particle size experiment on the Aeronomy of Ice in the Mesosphere spacecraft:

Atmospheric gravity waves as drivers for longitudinal variability in polar mesospheric cloud occurrence, J. Geophys. Res., 115, D13102, doi:10.1029/2009JD013185, 2010. 5655

Chu, X., Gardner, C. S., and Roble, R.: Lidar studies of interannual, seasonal and diurnal variations of polar mesospheric clouds at the South Pole, J. Geophys. Res., 108(D8), 8447, doi:10.1029/2002JD002524, 2003. 5644

DeLand, M. T., Shettle, E. P., Thomas, G. E., and Olivero, J. J.: Latitude-dependent long-term variations in polar mesospheric clouds from SBUV version 3 PMC data, J. Geophys. Res., 112, D10315, doi:10.1029/2006JD007857, 2007. 5644, 5657

Donahue, T. M., Guenther, B., and Blamont, J. E.: Noctilucent clouds in daytime: Circumpolar particulate layers near the summer mesopause, J. Atmos. Sci., 26, 1205–1209, 1972. 5643

Fiedler, J., Baumgarten, G., and von Cossart, G.: Mean diurnal variations of noctilucent clouds during 7 years of lidar observations at ALOMAR, Ann. Geophys., 23, 1175–1181, doi:10.5194/angeo-23-1175-2005, 2005. 5644, 5648, 5650, 5652, 5657

Fiedler, J., Baumgarten, G., and Lübken, F.-J.: NLC observations during one solar cycle above ALOMAR, J. Atmos. Solar Terr. Phys., 424–433, doi:10.1016/j.jastp.2008.11.010, 2009. 5644, 5646, 5648, 5650

Fogle, B. and Haurwitz, B.: Noctilucent clouds, Space Sci. Rev., 6, 279–340, doi:10.1007/BF00173768, 1966. 5643

Gadsden, M.: Noctilucent clouds, Journal of the British Astronomical Association, 99, 210–214, 1989. 5643

Gerding, M., Höffner, J., Rauthe, M., Singer, W., Zecha, M., and Lübken, F.-J.: Simultaneous observation of noctilucent clouds, mesospheric summer echoes, and temperature at a mid-latitude station (54° N), J. Geophys. Res., 112, D12111, doi:10.1029/2006JD008135, 2007. 5644

Hansen, G., Servazi, M., and von Zahn, U.: First detection of a noctilucent clouds by lidar, Geophys. Res. Lett., 16, 1445–1448, doi:10.1029/GL016i012p01445, 1989. 5645

Hartogh, P., Sonnemann, G. R., Grygalashvyly, M., Song, L., Berger, U., and Lübken, F.-J.: Water vapor measurements a ALOMAR over a solar cycle compared with model calculations by LIMA, J. Geophys. Res., 115, D00I17, doi:10.1029/2009JD012364, 2010. 5659

Hervig, M., Thompson, R. E., McHugh, M., Gordley, L. L., Russel III, J. M., and Summers, M. E.: First confirmation that water ice is the primary component of polar mesospheric clouds, Geophys. Res. Lett., 28, 971–974, doi:10.1029/2000GL012104, 2001. 5643

Höffner, J., Fricke-Begemann, C., and Lübken, F.-J.: First observations of noctilucent clouds by

lidar at Svalbard, 78° N, Atmos. Chem. Phys., 3, 1101–1111, doi:10.5194/acp-3-1101-2003, 2003. 5644

Jesse, O.: Auffallende Abenderscheinungen am Himmel, Meteorol. Zeitung, 2, 311–312, 1885. 5642

5   Jesse, O.: Die Höhe der leuchtenden Nachtwolken, Astron. Nachrichten, 140, 161–168, 1896. 5643

Kirkwood, S., Dalin, P., and Réchou, A.: Noctilucent clouds observed from the UK and Denmark - trends and variations over 43 years, Ann. Geophys., 26, 1243–1254, doi:10.5194/angeo-26-1243-2008, 2008. 5644

10   Klekociuk, A. R., Morris, R. J., and Innis, J. L.: First Southern Hemisphere common-volume measurement of PMC and PMSE, Geophys. Res. Lett., L24804, doi:10.1029/2008GL035988, 2008. 5644

Langer, M., Müller, K. P., and Fricke, K. H.: Rayleigh lidar detection of aerosol echoes from noctilucent cloud altitudes at the Arctic circle, Geophys. Res. Lett., 22, 381–384,
15   doi:10.1029/94GL02903, 1995. 5645

Leslie, R. C.: Sky glows, Nature, 32, p. 245, 1885. 5642

Lübken, F.-J.: Thermal structure of the arctic summer mesosphere, J. Geophys. Res., 104, 9135–9149, doi:10.1029/1999JD900076, 1999. 5652

Lübken, F.-J., Fricke, K. H., and Langer, M.: Noctilucent clouds and the thermal struc-
20   ture near the Arctic mesopause in summer, J. Geophys. Res., 101, 9489–9508, doi:10.1029/96JD00444, 1996. 5643

Lübken, F.-J., Rapp, M., and Strelnikova, I.: The sensitivity of mesospheric ice layers to atmospheric background temperatures and water vapor, Adv. Space Res., 40, 794–801, doi:10.1016/j.asr.2007.01.014, 2007. 5659

25   Lübken, F.-J., Berger, U., and Baumgarten, G.: Stratospheric and solar cycle effects on long-term variability of mesospheric ice clouds, J. Geophys. Res., D00I06, doi:10.1029/2009JD012377, 2009. 5659

Marsh, D. R., Garcia, R. R., Kinnison, D. E., Boville, B. A., Sassi, F., Solomon, S. C., and Matthes, K.: Modeling the whole atmosphere response to solar cycle changes in radia-
30   tive and geomagnetic forcing, J. Geophys. Res., 112, D23306, doi:10.1029/2002JD002364, 2007. 5652

Nussbaumer, V., Fricke, K. H., Langer, M., Singer, W., and von Zahn, U.: First simultaneous and common volume observations of noctilucent clouds and polar mesosphere summer echoes

by lidar and radar, J. Geophys. Res., 101, 19161–19167, doi:10.1029/96JD01213, 1996. 5645

Randel, W. J., Wu, F., Vömel, H., Nedoluha, G. E., and Forster, P.: Decreases in stratospheric water vapor after 2001: Links to changes in the tropical tropopause and the Brewer-Dobson circulation, J. Geophys. Res., 111, D12312, doi:10.1029/2005JD006744, 2006. 5657

Rapp, M. and Thomas, G. E.: Modeling the microphysics of mesospheric ice particles: Assessment of current capabilities and basic sensitivities, J. Atmos. Solar Terr. Phys., 68, 715–744, doi:10.1016/j.jastp.2005.10.015, 2006. 5643

Rapp, M., Lübken, F.-J., Müllemann, A., Thomas, G., and Jensen, E.: Small scale temperature variations in the vicinity of NLC: experimental and model results, J. Geophys. Res., 107, 4392, doi:10.1029/2001JD001241, 2002. 5655

Rauthe, M., Gerding, M., Höffner, J., and Lübken, F.-J.: Lidar temperature measurements of gravity waves over Kühlungsborn (54° N) from 1 to 105 km: A winter-summer comparison, J. Geophys. Res., 111, D24108, doi:10.1029/2006JD007354, 2006. 5652

Romejko, V. A., Dalin, P. A., and Pertsev, N. C.: Forty years of noctilucent cloud observations near Moscow: Data base and simple statistics, J. Geophys. Res., 108(D8), 8443, doi:10.1029/2002JD002364, 2003. 5643

Schmidt, H., Brasseur, G., Charron, M., Manzini, E., Giorgetta, M., Diehl, T., Fomichev, V., Kinnison, D., Marsh, D., and Walters, S.: The HAMMONIA chemistry climate model: sensitivity of the mesopause region to the 11-year cycle and CO_2 doubling, J. Climate, 19, 3903–3931, 2006. 5652

Shettle, E. P., DeLand, M. T., Thomas, G. E., and Olivero, J. J.: Long term variations in the frequency of polar mesospheric clouds in the Northern Hemisphere from SBUV, Geophys. Res. Lett., 36, L02803, doi:10.1029/2008GL036048, 2009. 5644, 5657

Singer, W., Keuer, D., and Eriksen, W.: The ALOMAR MF radar: Technical design and first results, in: Proceedings of the 13th ESA Symposium on European Rocket and Balloon Programmes and Related Research, Oeland, Sweden (ESA SP–397), edited by Kaldeich-Schürmann, B., ESA SP-397, 101–104, 1997. 5647

Stevens, M. H., Siskind, D. E., Eckermann, S. D., Coy, L., McCormack, J. P., Englert, C. R., Hoppel, K. W., Nielsen, K., Kochenash, A. J., Hervig, M. E., Randall, C. E., Lumpe, J., Bailey, S. M., Rapp, M., and Hoffmann, P.: Tidally induced variations of polar mesospheric cloud altitudes and ice water content using a data assimilation system, J. Geophys. Res., 115, D18209, doi:10.1029/2009JD013225, 2010. 5656

Thayer, J. P., Rapp, M., Gerrard, A. J., Gudmundsson, E., and Kane, T. J.: Gravity wave influences on Arctic mesospheric clouds as determined by a Rayleigh lidar at Sondrestrom, Greenland, J. Geophys. Res., 108(D8), 8449, doi:10.1029/2002JD002363, 2003. 5644

Thomas, G. E., McPeters, R. D., and Jensen, E. J.: Satellite observations of polar mesospheric
5   clouds by Solar Backscattered Ultraviolet spectral radiometer: Evidence of a solar cycle dependence, J. Geophys. Res., 96, 927–939, doi:10.1029/90JD02312, 1991. 5643

Thomas, G. E., Olivero, J. J., DeLand, M., and Shettle, E. P.: A response to the article by U. von Zahn, "Are noctilucent clouds truly a "miner's canary" for global change?", Trans. Am. Geophys. Union (EOS), 84, 352–553, doi:10.1029/2003EO360008, 2003. 5644

10 Turco, R. P., Toon, O. B., Whitten, R. C., Keesee, R. G., and Hollenbach, D.: Noctilucent clouds: Simulation studies of their genesis, properties and global influences, Planet. Space Sci., 30, 1147–1181, doi:10.1016/0032-0633(82)90126-X, 1982. 5643

Vestine, E. H.: Noctilucent clouds, J. of the Royal Astronomical Society of Canada, 18, 249–272, 303–317, 1934. 5643

15 von Cossart, G., Fiedler, J., and von Zahn, U.: Size distributions of NLC particles as determined from 3-color observations of NLC by ground-based lidar, Geophys. Res. Lett., 26, 1513–1516, doi:10.1029/1999GL900226, 1999. 5644

von Zahn, U.: Are noctilucent clouds truly a "miner's canary" for global change?, Trans. Am. Geophys. Union (EOS), 84, 261–264, doi:10.1029/2003EO280001, 2003. 5644

20 von Zahn, U., von Cossart, G., Fiedler, J., Fricke, K. H., Nelke, G., Baumgarten, G., Rees, D., Hauchecorne, A., and Adolfsen, K.: The ALOMAR Rayleigh/Mie/Raman lidar: objectives, configuration, and performance, Ann. Geophys., 18, 815–833, doi:10.1007/s00585-000-0815-2, 2000. 5645

Wegener, A.: Die Erforschung der obersten Atmosphärenschichten, Gerlands Beiträge zur
25 Geophysik, 11, 104–124, 1912. 5643

Witt, G.: Height, structure and displacements of noctilucent clouds, Tellus, 14, 1–18, 1962. 5643

Title Page

Abstract | Introduction

Conclusions | References

Tables | Figures

◄ | ►

◄ | ►

Back | Close

Full Screen / Esc

Printer-friendly Version

Interactive Discussion

Table 1. Correlation between seasonal mean NLC parameters, solar activity and temperature at 83 km altitude for clouds above the long-term limit ($\beta_{max} > 4$). Numbers are for the whole time series and reduced data sets (in brackets): Lyman-α dependencies without 2005–2008, temperature dependencies without 1998. Units: occurrence [%], brightness [$10^{-10}\,\text{m}^{-1}\,\text{sr}^{-1}$], altitude [km], Lyman-$\alpha$ [$10^{11}\,\text{photons}\,\text{s}^{-1}\,\text{cm}^{-1}$], temperature [K]. Lyman-α data are taken from http://lasp.colorado.edu/lisird/lya/. Temperatures are calculated by LIMA for times of lidar measurements. Slopes for the linear regressions are only given for significant correlations.

X	Y	Corr. Coeff.	Signif.	Slope
Occurrence	Lyman-α	−0.28 (−0.73)	(95%)	(−7.92)
Brightness (β_{max})	Lyman-α	−0.54 (−0.73)	95% (95%)	−1.49 (−2.18)
Altitude (z_c)	Lyman-α	+0.58 (+0.68)	95% (95%)	+0.25 (+0.28)
Occurrence	T(83 km)	−0.63 (−0.77)	95% (99%)	−3.80 (−5.87)
Brightness (β_{max})	T(83 km)	−0.27 (−0.20)		
Altitude (z_c)	T(83 km)	+0.43 (+0.62)	(95%)	(+0.19)

Full Screen / Esc

Printer-friendly Version

Interactive Discussion
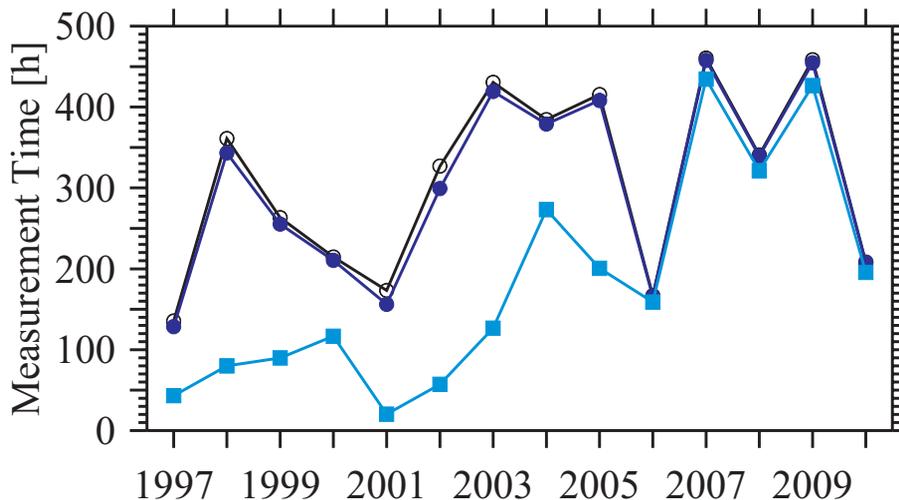
Fig. 1. Measurement times of the ALOMAR RMR-lidar during the NLC season (1 June–15 August) for different data sets: entire (black hollow circles), long-term (blue filled circles) and high-sensitivity (light blue filled squares). The last two data subsets contain only measurements with mean uncertainties of $\Delta\beta_{\mathrm{NLC}}(z) < 4\times10^{-10}\,\mathrm{m}^{-1}\,\mathrm{sr}^{-1}$ and $\Delta\beta_{\mathrm{NLC}}(z) < 1\times10^{-10}\,\mathrm{m}^{-1}\,\mathrm{sr}^{-1}$, respectively, in the altitude range from 80 to 90 km.
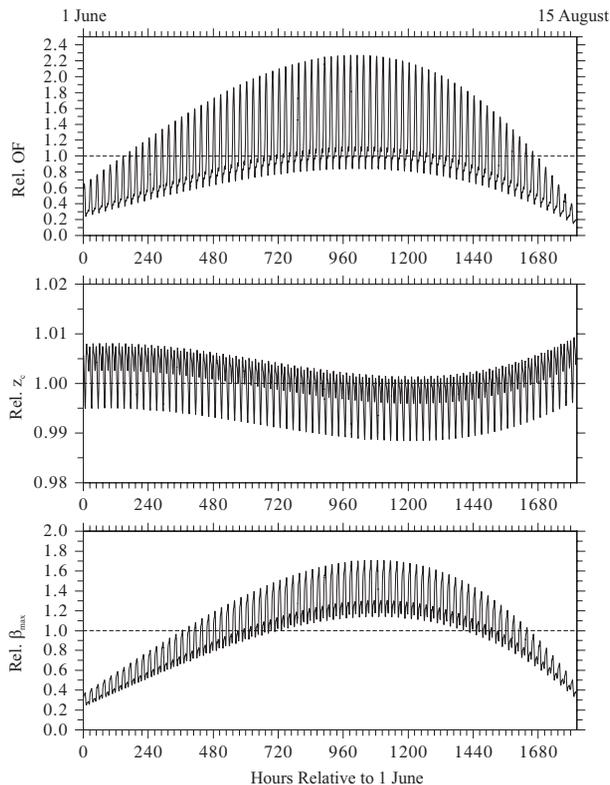
Fig. 2. Hourly relative variations of NLC occurrence (top), altitude (middle) and brightness (bottom) as determined from fit coefficients for the integrated ALOMAR RMR-lidar data set from 1997 to 2010. For details see text.
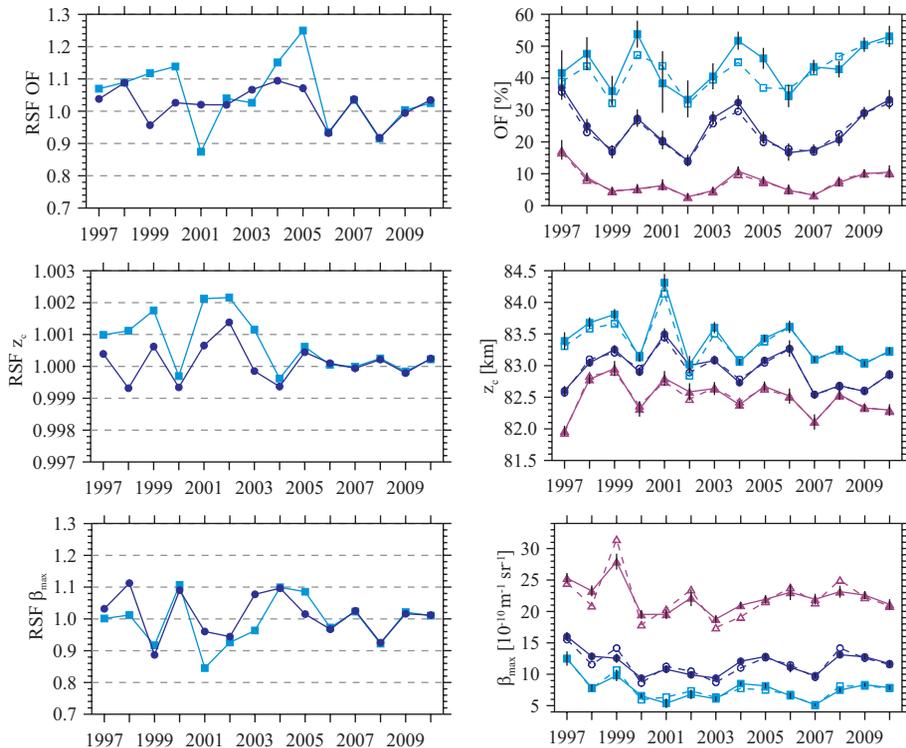
Fig. 3. Seasonal mean relative sampling factors RSF (left) and mean values (right) of NLC occurrence (top), altitude (middle) and brightness (bottom). Sampling curves are calculated for two data sets: long-term (blue circles) and high-sensitivity (light blue squares). Curves at the right side are for three brightness classes: $\beta_{max} > 1$ (light blue squares), $\beta_{max} > 4$ (blue circles), $\beta_{max} > 13$ (purple triangles). Dashed lines and open symbols are corrected regarding the sampling quality. Vertical bars indicate confidence limits for the occurrence at 95%-level and errors of the means for altitude and brightness.

Title Page

Abstract | Introduction

Conclusions | References

Tables | Figures

|◄ | ►|

◄ | ►

Back | Close

Full Screen / Esc

Printer-friendly Version

Interactive Discussion
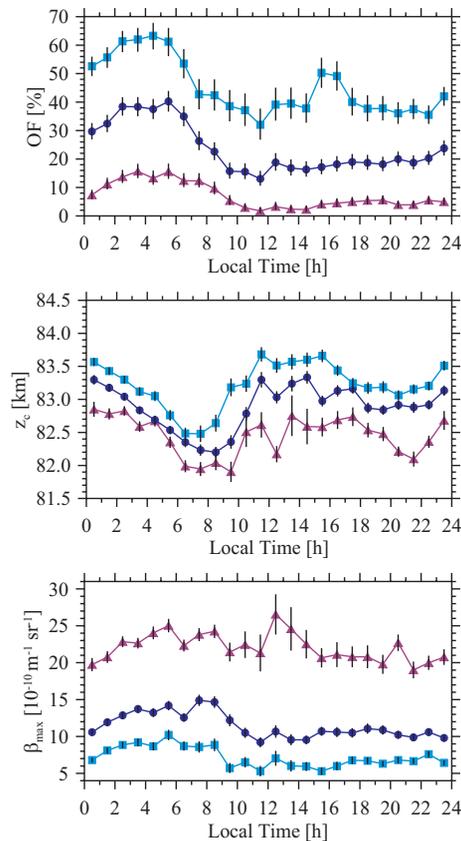
Fig. 4. Diurnal variation of NLC occurrence (top), altitude (middle) and brightness (bottom) for the integrated data set from 1997 to 2010, sorted by brightness classes: $\beta_{max} > 1$ (light blue squares), $\beta_{max} > 4$ (blue circles), $\beta_{max} > 13$ (purple triangles). Vertical bars indicate confidence limits for the occurrence at 95%-level and errors of the means for altitude and brightness.

Title Page

Abstract | Introduction

Conclusions | References

Tables | Figures

◄◄ | ►►

◄ | ►

Back | Close

Full Screen / Esc

Printer-friendly Version

Interactive Discussion
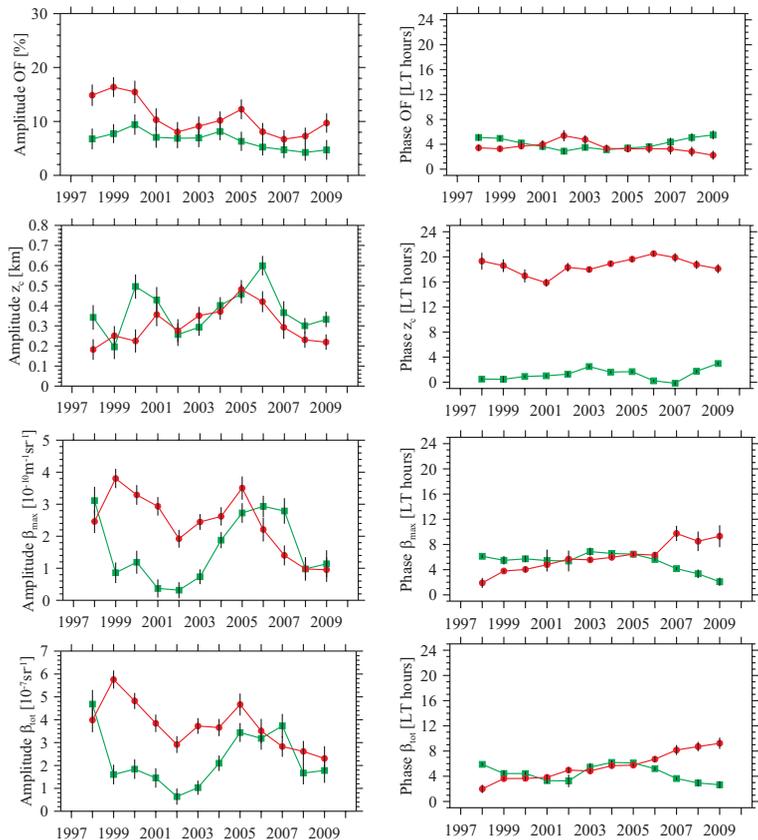
Fig. 5. Year-to-year variations of seasonal mean amplitudes and phases for 24- (red circles) and 12-hour (green squares) periods of NLC parameters. From top to bottom: occurrence, altitude, brightness (β_{max}), brightness (β_{tot}). Based on 3 years running means for clouds above the long-term limit. Vertical bars are errors resulting from Levenberg-Marquardt least-squares fits.

ACPD

11, 5641–5679, 2011

NLC and background atmosphere

J. Fiedler et al.

Title Page

Abstract | Introduction

Conclusions | References

Tables | Figures

◄ | ►◄

◄ | ►

Back | Close

Full Screen / Esc

Printer-friendly Version

Interactive Discussion
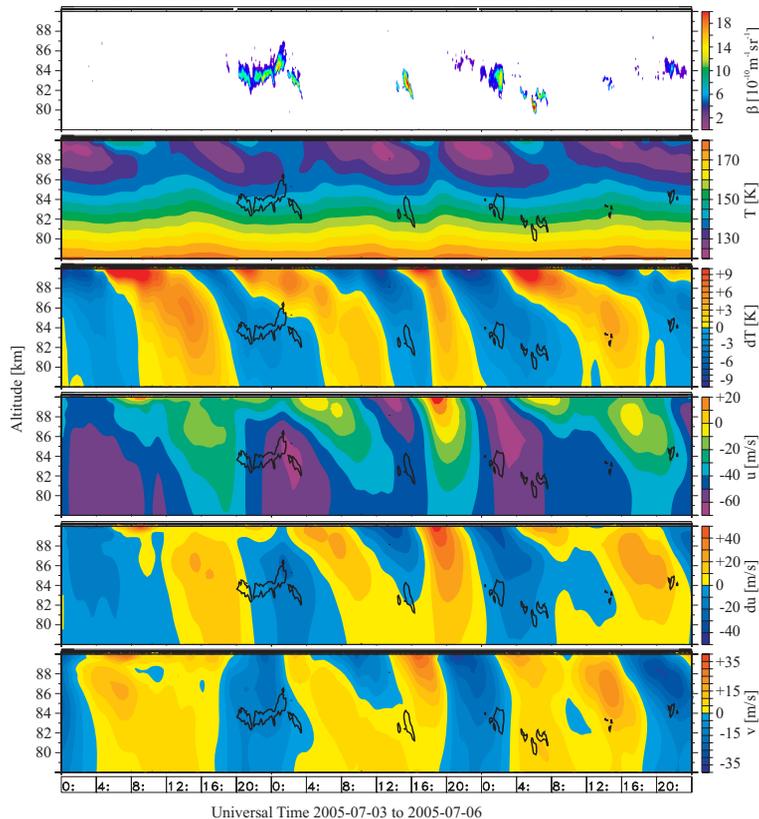
Fig. 6. Time series for NLC (measured by RMR-lidar) and atmospheric parameters (calculated by LIMA-model) for three consecutive days (3–5 July 2005) above ALOMAR. From top to bottom: NLC brightness in terms of volume backscatter coefficient, temperature, temperature deviation, zonal wind, zonal wind deviation, and meridional wind. Deviations are calculated with respect to the mean profiles over the whole time period. NLC contours for a brightness of $\beta_{max} = 4$ are plotted on top of the LIMA results.

Title Page

Abstract | Introduction

Conclusions | References

Tables | Figures

◄ | ►

◄ | ►

Back | Close

Full Screen / Esc

Printer-friendly Version

Interactive Discussion
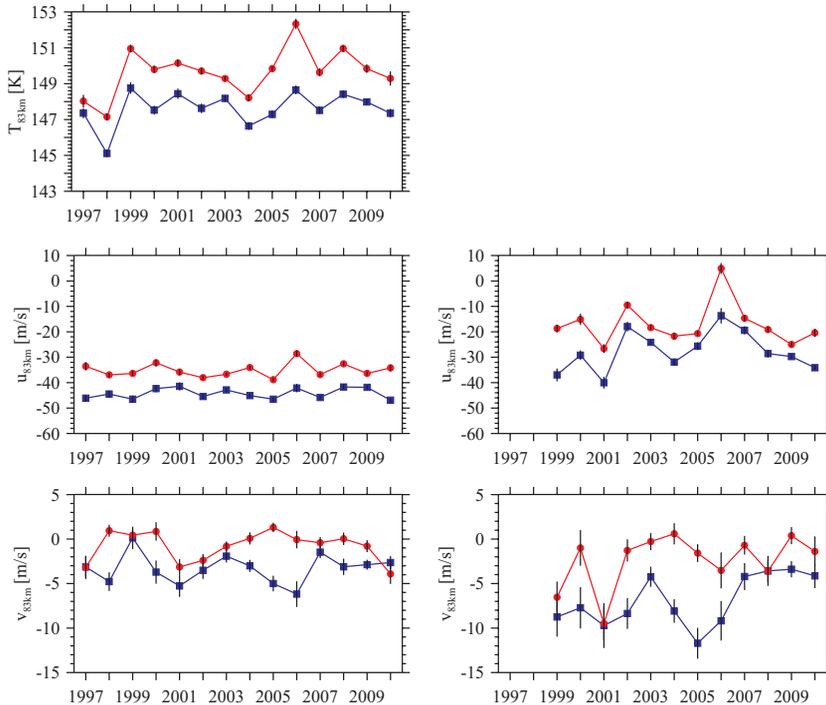
Fig. 7. Seasonal mean temperature (top), zonal (middle) and meridional (bottom) wind at 83 km altitude above ALOMAR as calculated by the LIMA-model (left) and measured by the ALOMAR MF-radar (right). Data are based on hourly mean values. Only hours with ALOMAR RMR-lidar measurements are taken into account (long-term data set). Data are separated for confirmed absence (red circles) and presence ($\beta_{max} > 4$, blue squares) of NLC. Vertical bars are error of the means.

Title Page

Abstract | Introduction

Conclusions | References

Tables | Figures

◄ | ►

◄ | ►

Back | Close

Full Screen / Esc

Printer-friendly Version

Interactive Discussion
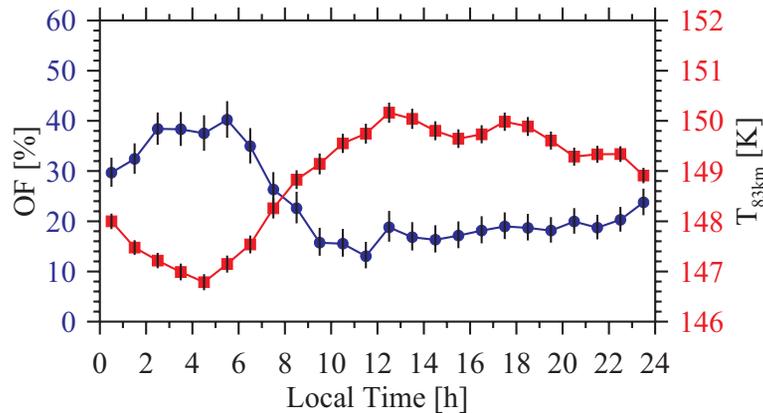
Fig. 8. Diurnal variation of NLC occurrence determined from ALOMAR RMR-lidar ($\beta_{max} > 4$, blue circles) and temperature at 83 km altitude during times of lidar measurements as calculated by LIMA (red squares) for the integrated data set from 1997 to 2010. Vertical bars indicate confidence limits for the occurrence at 95%-level and errors of the mean temperatures.
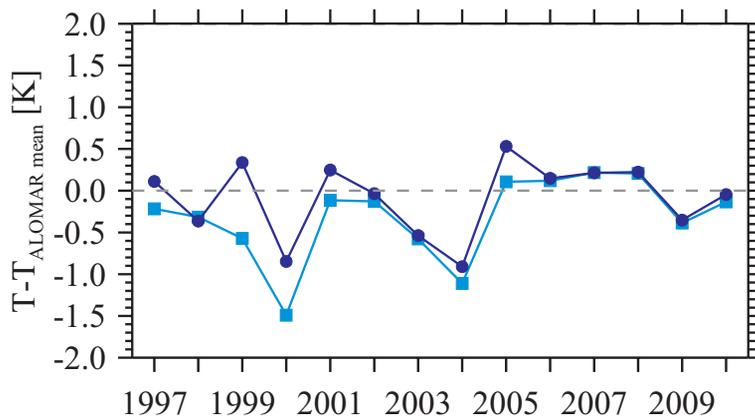
Fig. 9. Seasonal mean sampling of temperature at 83 km altitude during ALOMAR RMR-lidar measurements as determined by LIMA. Temperatures calculated solely for hours with lidar measurements are compared to entire means from 1 June to 15 August. Sampling curves are calculated for two data sets: long-term (blue circles) and high-sensitivity (light blue squares).

Full Screen / Esc

Printer-friendly Version

Interactive Discussion

Fig. 10. Reconstructed NLC occurrence time series from 24- and 12-hours harmonic oscillations. Phases are taken from Fig. 5 for the upper plots and fixed to 1997 values for the lower plots. The mean variation over all 14 years is given by the tick line. The right panels show the year-to-year variations resulting from the diurnal variations of the left panels. Local times for NOAA-16/17/18 overpasses of ALOMAR are shown in colors: 4 LT (blue circles), 12 LT (green squares), 21 LT (red triangles). Black curves/asterisks are the mean over all local times. Based on 3 years running means for clouds above the long-term limit.
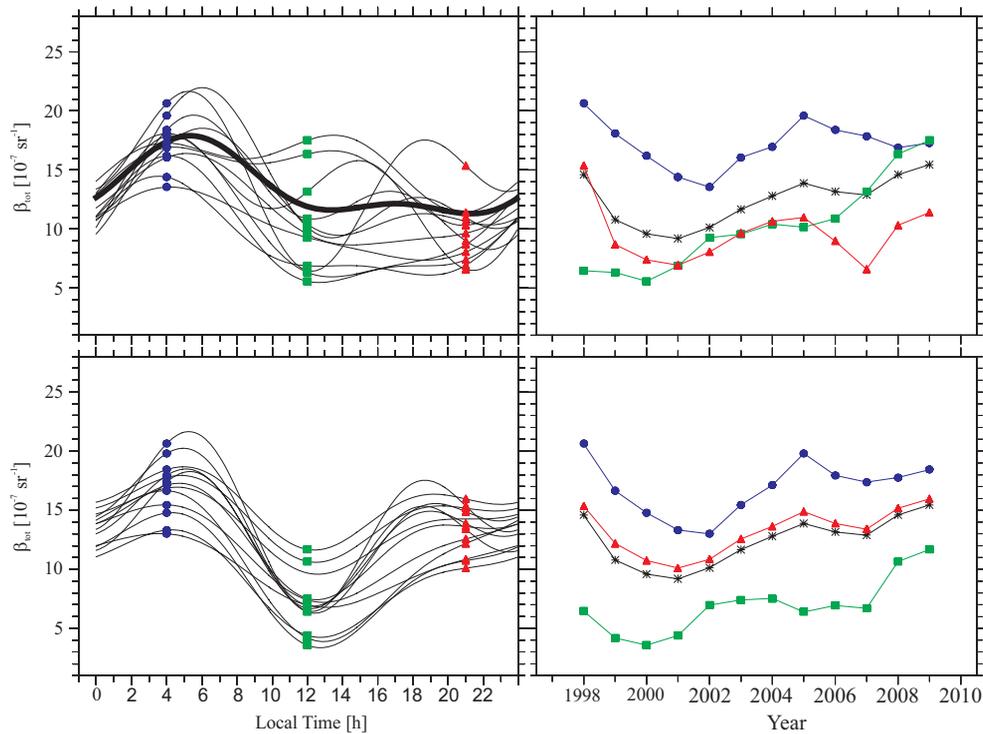
Fig. 11. Same as Fig. 10, but for NLC brightness (β_{tot}).

Title Page

Abstract | Introduction

Conclusions | References

Tables | Figures

|◀ | ▶|

◀ | ▶

Back | Close

Full Screen / Esc

Printer-friendly Version

Interactive Discussion

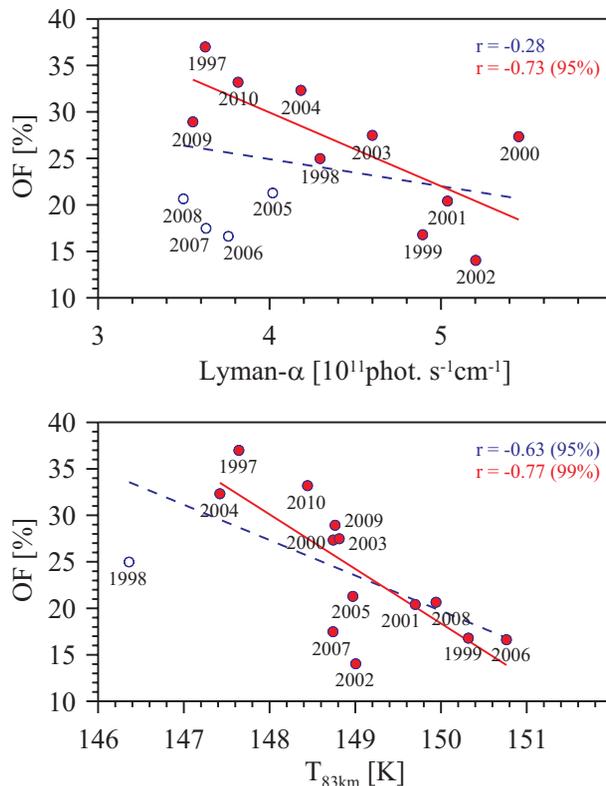**Fig. 12.** Occurrence of NLC above the long-term limit ($\beta_{max} > 4$) at ALOMAR as function of solar activity (top) and temperature at 83 km altitude (bottom). Lyman-α data are taken from http://lasp.colorado.edu/lisird/lya/ and averages over the NLC season (1 June–15 August). Temperatures are calculated by LIMA for times of lidar measurements. Blue colors/dashed lines represent the whole data set covering 14 years, whereas the outlier adjusted data subsets are indicated in red/solid lines. Significance levels of the correlation coefficients are given in brackets.